

# How to Design a Three-Stage Architecture for Audio-Visual Active Speaker Detection in the Wild

Okan Köpüklü<sup>1</sup>, Maja Taseska<sup>2</sup>, Gerhard Rigoll<sup>1</sup>

<sup>1</sup> Technical University of Munich

<sup>2</sup> Microsoft

## Abstract

Successful active speaker detection requires a three-stage pipeline: (i) audio-visual encoding for all speakers in the clip, (ii) inter-speaker relation modeling between a reference speaker and the background speakers within each frame, and (iii) temporal modeling for the reference speaker. Each stage of this pipeline plays an important role for the final performance of the created architecture. Based on a series of controlled experiments, this work presents several practical guidelines for audio-visual active speaker detection. Correspondingly, we present a new architecture called ASDNet, which achieves a new state-of-the-art on the AVA-ActiveSpeaker dataset with a mAP of 93.5% outperforming the second best with a large margin of 4.7%. Our code and pretrained models are publicly available <sup>1</sup>.

## 1. Introduction

Fusion of audio and video modalities has been shown to provide promising solutions to long-standing challenging problems. These include among others, speaker diarization [16], biometrics [7], and action recognition [15, 38]. Similar to other tasks, Audiovisual Active Speaker Detection (AV-ASD) has also long been studied in literature [9, 10]. A particularly challenging flavor of this problem is AV-ASD in the wild, where speech is to be detected and assigned to one of possibly multiple active speakers at each instant in time. Clearly, fusing the complementary discriminative information from audio and video modalities is crucial: visual-only approaches can easily be mistaken by other face/mouth motions such as eating, yawning or emotional expressions. Audio-only approaches, although able to perform source clustering and separation [18, 46], aren't sufficiently robust to count number of speakers and assign speech to the correct source. This is especially challenging with a single microphone input in acoustically adverse conditions, typically encountered in practice.

<sup>1</sup><https://github.com/okankop/ASDNet>

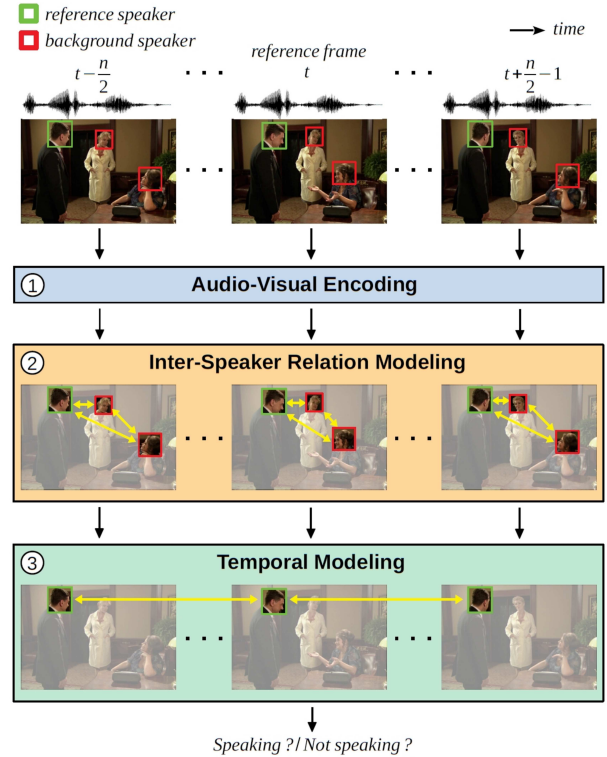


Figure 1. Audio-visual active speaker detection pipeline. The task is to determine if the reference speaker at frame  $t$  is *speaking* or *not-speaking*. The pipeline starts with audio-visual encoding of each speaker in the clip. Secondly, inter-speaker relation modeling is applied within each frame. Finally, temporal modeling is used to capture long-term relationships in natural conversations. Examples are from AVA-ActiveSpeaker dataset [42].

Recently, the AVA-ActiveSpeaker dataset [42] has provided the first large-scale standard benchmark for the task of audio-visual active speaker detection in the wild. Recent research [1, 32] indicates that active speaker detection in the wild requires (i) integration of audio-visual information for each speaker, (ii) contextual information that captures inter-speaker relationships, and (iii) temporal modeling to exploit long term relationship in natural conversation. In this pa-

per, we consolidate this three-stage pipeline for audio-visual speaker detection, illustrated in Fig. 1, and study the importance of each stage in detail.

**Contributions.** We propose a novel three-stage pipeline for audio-visual active speaker detection in the wild. Our architecture, named ASDNet, sets a new state-of-the-art result on AVA-ActiveSpeaker dataset with a 93.5% mAP, and outperforms the second best method [32] with a large margin of 4.7% mAP (Section 4.5).

With the hope to contribute valuable guidelines for future research in this domain, we cover in detail the importance, the motivation, and the design for each stage. More concretely:

- (1) We discuss suitable architectures and configurations for feature encoding of raw audio-visual data for each individual speaker (Section 3.2).
- (2) We propose a simple yet effective inter-speaker relation modeling mechanism and compare its performance with previously proposed approaches (Section 3.3 and 4.2).
- (3) We analyze various Recurrent Neural Network (RNN) architectures for temporal modelling and compare their contribution to final system performance (Section 3.4 and 4.3).

## 2. Related Work

We present the related work in two parts: (i) audio-visual feature extraction in various applications, and (ii) contributions that address active speaker detection in the wild and its challenges.

### 2.1. Audio-visual feature extraction

**Audio.** A common approach to extract features in speech and audio research in different applications, is to use Convolutional Neural Networks (CNNs) and RNNs with log-Mel or Short-Time Fourier Transform (STFT) spectrograms as inputs [13]. The popularity of these fixed transforms is due to their success in traditional speech and audio processing and the fact that they extract relevant information from first principles. Furthermore, the image-like configuration of the spectrograms allows to employ network architectures well-known from computer vision applications. Particularly, in AV-ASD, this allows to use similar audio and video backbone architectures [1, 32].

Based on the interpretation of CNNs as a data-driven filterbank, researchers have applied CNNs directly on the audio waveforms to capture discriminative information for the task at hand [12, 30]. Such approach in the context of AV-ASD has been used for an audio backbone in [2]. However, these approaches need much more data and computational resources than the ones exploiting spectrograms. With the goal to exploit the best from both worlds, researchers have come up with learnable, but yet constrained transformations of raw audio data. Examples include Harmonic

CNNs used for music tagging, and the SincNet architecture proposed in [41]. The latter was successfully used in several audio applications [27, 33, 36]. To our best knowledge, this promising architecture hasn’t been used in the context of AV-ASD.

**Video.** Active speaker detection using only video modality can be viewed as action recognition task. Prior to CNNs, action recognition research was dominated by hand-crafted features [28, 29, 49], combined with Fisher Vector representations [39] or Bag-of-Features histograms [8]. Ever since AlexNet [26] won the ImageNet Challenge [43], hand-crafted features were mostly abandoned in favor of features extracted by CNNs. This trend extended to video analysis tasks as well, including action recognition. Initially, due to the absence of a large-scale video dataset, architectures for action recognition could benefit from pretraining on the very-large ImageNet dataset [11]. The first intuitive approach was to treat video frames as multi channel input to 2D-CNNs [21, 45]. Other approaches include extraction of frame-level features with a 2D-CNN, followed by a spatiotemporal modeling mechanism [23].

With the availability of large-scale video datasets such as Kinetics [3], Moments-in-Time [37], and Jester [34], 2D-CNNs were replaced by 3D-CNNs, to better capture temporal information and motion patterns within video frames. A 3D-CNN architecture was first proposed in [20] by Ji *et al.* Since then, many 3D-CNN architectures for video recognition tasks followed, such as C3D [47], I3D [3], P3D [40], R(2+1)D [48], SlowFast [14], etc. In [17], the effect of dataset size on performance is investigated for several 3D-CNN architectures. Inflated versions of popular resource-efficient 2D-CNN architectures are analyzed for video classification tasks in [24]. In this work, we use the variants of 3D-CNNs for the AV-ASD task.

**Fusion.** The extracted modality-specific features can be combined at data level [25], feature level [35] or decision level [45]. The fusion that we have applied in this work can be considered as feature level fusion since we keep processing fused features at inter-speaker relation modeling and temporal modeling mechanisms afterwards.

### 2.2. Active speaker detection in the wild

Audio-visual active speaker detection is a specific case of source separation [4, 50], where audio and visual signals are leveraged jointly to assign a speech segment to its speaker. For this task, initial approaches [9, 10] work on datasets, which are collected at controlled environments. With the availability of AVA-ActiveSpeaker dataset [42], the research community could eventually shifted towards speaker detection in the wild.

Audio-visual feature extraction and fusion is the first step in all top-performing frameworks for active speaker detec-

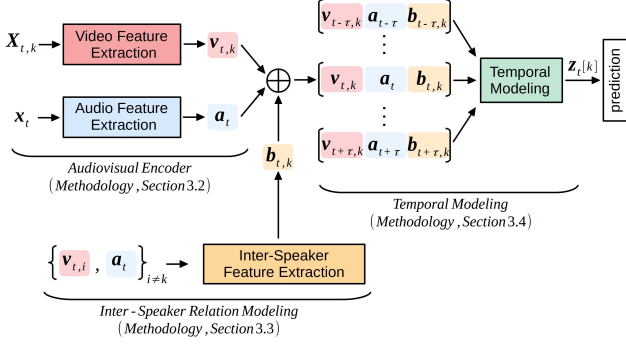


Figure 2. Overview of the proposed three-stage pipeline.

tion in the wild [1, 6, 32, 42, 54]. A two-backbone modality approach has established itself as standard architecture due to its versatility [45]. With a good choice of audio-visual feature extraction, and temporal modelling with a RNNs, the authors in [6] were able to achieve competitive performance on the AVA-ActiveSpeaker dataset. Often neglected is the context information that can be obtained by modelling inter-speaker relationships. Only very recently researchers have shown the importance of this aspect, and proposed methods to exploit the context information [1, 32]. Temporal modeling, usually with RNNs, has also been an inseparable part of the active speaker detection pipeline [1, 6, 42, 54].

### 3. Methodology

Drawing inspiration from the major insights from recent research, outlined in Section 2.2, we seek to establish a general pipeline that incorporates audio-visual encoding, inter-speaker (context) modelling, and temporal modelling. Following this methodology and choosing appropriate architectures for each component, we are able to exceed the current state-of-the-art performance on the AVA-ActiveSpeaker dataset.

#### 3.1. Notation and Overview

Let  $K$  denote the total number of speakers in a given clip. The data available to the active speaker detection system at time  $t$  is a set  $\mathcal{X}_t = \{X_{t,1}, X_{t,2}, \dots, X_{t,K}, x_t\}$ , where  $X_{t,k} \in \mathbb{R}^{n \times 3 \times d_h \times d_w}$  is a tensor of face crops corresponding to the  $k$ -th speaker. The height and width of the face crops are denoted by  $d_h$  and  $d_w$ , 3 is the RGB channels and  $n$  is the number of consecutive face crops centering time  $t$ . The vector  $x_t$  contains the samples of the audio track corresponding to the duration of the video input. Given the input data, the objective of an active speaker detection system is to produce a binary vector  $z_t$ , where  $z_t[k] = 1$  if the  $k$ -th speaker is detected as *speaking* at time frame  $t$ , and  $z_t[k] = 0$  otherwise.

A high-level overview of our pipeline that maps the raw data  $\mathcal{X}_t$  to the predictions  $z_t$  is illustrated in Fig. 2. Next, in

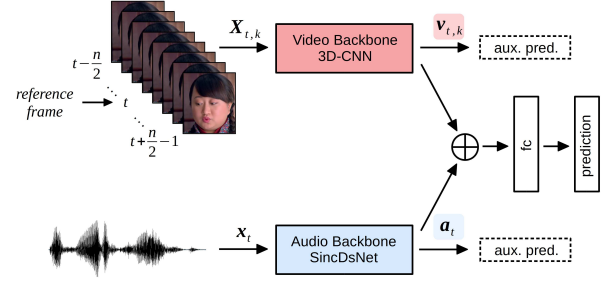


Figure 3. Audio-visual encoder architecture. Visual input  $X_{t,k}$  and audio input  $x_t$  are fed to the respective backbones to produce features  $v_{t,k}$  and  $a_t$ . A concatenated feature vector  $v_{t,k} \oplus a_t$  is fed to a fully connected layer which produces a prediction if speaker  $k$  is speaking at time  $t$ . Prediction heads are removed after training and are not part of the global picture in Fig. 2.

Sec. 3.2-3.4, we zoom in on the design of the three pipeline components. In Sec. 3.5, we discuss the training strategy that enables an end-to-end inference: from face crops and an audio waveform, to a prediction *speaking* or *not speaking* for each speaker in the video clip.

#### 3.2. Audio-Visual Encoder Architecture

Our audio-visual encoder is illustrated in Fig. 3. The stack of face thumbnails  $X_{t,k}$  consists of  $n$  frames,  $X_{t-\frac{n}{2},k}, \dots, X_{t,k}, \dots, X_{t+\frac{n}{2}-1,k}$ , and the size of the audio input vector  $x_t$  is determined by the number of video frames, the frame rate of the video signal, and the sampling rate of the audio signal. The encoder produces an embedding vector by concatenating the following modality-specific embeddings

$$v_{t,k} = f_v(X_{t,k}; w_v), \quad a_t = f_a(x_t; w_a). \quad (1)$$

The embedding functions  $f_v$  and  $f_a$  are neural networks with trainable parameters  $w_v$  and  $w_a$ , respectively, which will be discussed shortly.

The concatenated features  $v_{t,k} \oplus a_t$  are fed into a fully connected layer to get final predictions. To train the audio-visual encoder, we apply cross-entropy loss between the predictions and ground-truth labels. To ensure that consistent discriminative features will be extracted from both modalities, we apply auxiliary classification networks after each backbone, following previous works [1, 32, 42]. The auxiliary networks are also trained with cross-entropy loss. The final loss becomes  $L_{final} = L_{av} + L_a + L_v$ . After training is completed, supervision heads are discarded and only the audio-visual backbone is used to extract features  $v_{t,k}$  and  $a_t$  for all speakers and time instants.

In the remaining part of this section, we dive into the details of the video and audio backbones.

**Video backbone.** Different from majority of state-of-the-art approaches [1, 6, 32, 42, 54] that apply 2D-CNN as

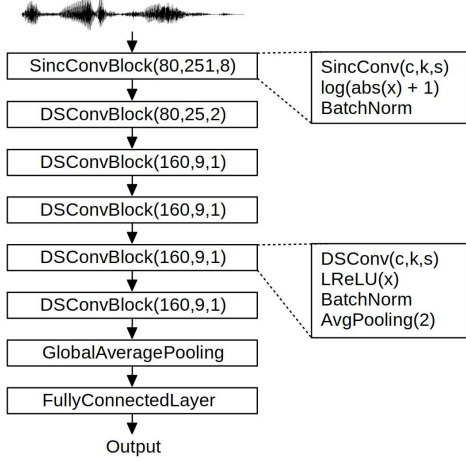


Figure 4. Audio feature encoding backbone utilizing Sinc Convolutions (SincConv) and Depthwise Separable Convolutions (DSConv). Convolution parameters are given as  $c, k, s$  representing the number of output channels, kernel size and applied stride, respectively.

video backbone, we apply a 3D-CNN as  $f_v$ . Our objective when choosing 3D-CNN was to benefit from its ability to capture motion patterns in face crops. Capturing motion patterns is crucial since movements of facial muscles and mouth are indicative of active speaking. We experimented with several high-performance and resource-efficient 3D-CNN architectures [24]. 3D-ResNeXt-101 performs best and becomes our final choice as video backbone. For all architectures, features before the fully connected layer are extracted as the video features  $\mathbf{v}_{t,k}$ .

**Audio backbone.** For the audio encoding backbone, the majority of existing AV-ASD approaches [1, 6, 32, 42, 54] extract Mel Frequency Cepstral Coefficients (MFCC) from the raw signal, and use the MFCCs as input to 2D-CNNs. In contrast, we propose an audio backbone architecture that directly operates on raw audio signal via sinc convolutions [41]. After sinc convolutions, we apply log-compression, i.e.,  $y = \log(\text{abs}(x) + 1)$ . This non-linearity has been effective in other raw audio processing tasks as well [27, 53]. The features extracted by the sinc-convolution block are used as input to Depthwise Separable Convolutional (DSConv) blocks with Leaky-ReLU nonlinearity [52]. The full audio encoder architecture, referred to as SincDSNet in the rest of the paper, is shown in Fig. 4. Features after the global average pooling are extracted as the audio features  $\mathbf{a}_t$ .

### 3.3. Inter-Speaker Relation Modeling (ISRM)

The audio-visual encoder described in the previous section, extracts features from each individual speaker separately. The features for speaker  $k$  do not contain any visual information from the remaining speakers in the frame.

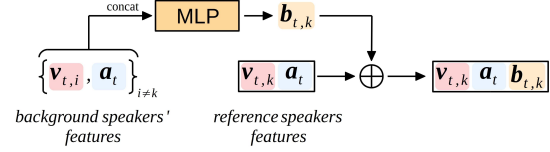


Figure 5. Inter-speaker relation modeling architecture. For reference speaker  $k$  at time instant  $t$ , we extract background features  $\mathbf{b}_{t,k}$  by passing the concatenated features of background speakers through one layer MLP. Extracted features are then concatenated to reference speakers video features and audio features.

However, features belonging to background speakers contain complementary information that improves the prediction performance [1]. As a part of our system, we propose a simple yet effective mechanism to aggregate information from the background speakers.

Consider a reference speaker  $k$  and  $m$  background speakers in the scene at time  $t$ . The output of the audio-visual encoder for the reference speaker is  $[\mathbf{v}_{t,k}, \mathbf{a}_t]$ . To incorporate information from background speakers,  $[\mathbf{v}_{t,k}, \mathbf{a}_t]$  is concatenated with an additional feature vector  $\mathbf{b}_{t,k}$ , as illustrated in Fig. 5. The vector  $\mathbf{b}_{t,k}$  is the output of a single-layer MLP whose inputs are the concatenated audio-visual embeddings from all background speakers at time  $t$ . Note that the number  $m$  is fixed from the system’s perspective: if there are less than  $m$  background speakers at time  $t$ , the encoder features are populated with zero vectors. If there are more than  $m$  speakers, only  $m$  are randomly selected. In this manner, the input dimension of the MLP is fixed, and the feature vector  $[\mathbf{v}_{t,k}, \mathbf{a}_t, \mathbf{b}_{t,k}]$  is fed to the temporal modeling mechanism, described next.

### 3.4. Temporal Modeling

Speaking is a coherent action in time. In other words, if a person is speaking in previous time instants or future time instants, it is likely that the person is also speaking at the current time instant. This is also valid for *remaining silent* action. Therefore, temporal modeling is crucial for a successful active speaker detection architecture.

We experimented with several RNN-based temporal modeling architectures: Long Short-Term Memory (LSTM) [19], Gated Recurrent Unit (GRU) [5], Simple Recurrent Unit (SRU) [31] and their bidirectional versions. For the uni-directional methods, the reference frame is at the end of the input, while for the bidirectional methods it is at center of the input. The hidden state vector of the recurrent block at the reference frame is fed to a fully connected layer to produce a binary output  $\mathbf{z}_t[k] \in \{0, 1\}$  (i.e. active speaker or not). In case speakers’ features are not available for the selected time window, similar to [1] we apply same padding to the beginning or to the end. Out of all methods, Bidirectional-GRU performs best and becomes our final choice in temporal modeling stage.



Audio Backbone	Video Backbone	mAP
2D-ResNet-18	2D-ResNet-18	79.0
2D-ResNet-18	3D-ResNet-18	83.9
SincDSNet	2D-ResNet-18	80.8
SincDSNet	3D-ResNet-18	<b>86.1</b>

Table 1. Performance comparison of different audio and video backbones. Input length of 8-frames is used for all evaluations.

Audio Backbone	Params	MFLOP
SincDSNet	0.15M	13.8
2D-ResNet-18	11.2M	19.2

Table 2. Comparison of different audio backbones in terms of computational complexity and number of parameters.

### 3.5. Training Details

**Training Audio-Visual Encoding Backbones.** We train our audio-visual encoder using ADAM optimizer [22] for 70 epochs. Batch size is selected as highest possible number that fits to a single NVIDIA Titan XP GPU for different backbones. However, gradients are accumulated reaching to effective batch size of 192 before doing backward propagation. The learning rate is initialized with  $3 \times 10^{-4}$  and dropped by a factor of 10 at every 30 epochs. For video input, we apply random cropping, random horizontal flipping and color transformations as data augmentation at the training time. Finally, video input is reshaped to the resolution of  $160 \times 160$ . Audio data is extracted with sampling rate of 16 kHz. All 3D CNNs are pretrained on Kinetics [3], 2D CNNs are pretrained with ImageNet [11] and SincDSNet is trained from scratch. Once the training is finished, prediction heads are discarded and the features  $\mathbf{v}_{t,k} \in \mathbb{R}^{512}$  and  $\mathbf{a}_t \in \mathbb{R}^{160}$  are used for the training of ISRM and temporal modeling stages.

**Training ISRM and Temporal Modeling.** We have again used ADAM optimizer with cross-entropy loss to train ISRM and temporal modeling stages. We train with batch size of 256 and for 10 epochs. Learning rate is initialized with  $3 \times 10^{-6}$  and dropped by 10 at 5th epoch. For ISRM, MLP creates the feature  $\mathbf{b}_{t,k} \in \mathbb{R}^{128}$  independent from the number of background speaker features used. For RNN blocks, we always used two recurrent layers with hidden state dimension of 128, which experimentally proved to be working best.

Our final architecture ASDNet is implemented in PyTorch and all experiments are performed using a single NVIDIA Titan Xp GPU.

	Video Backbone	Params	GFLOP	mAP
32-f	3D-ResNeXt-101	48.6M	13.2	<b>88.9</b>
	3D-ResNet-18	33.2M	10.3	87.4
16-f	3D-ResNeXt-101	48.6M	14.1	<b>88.9</b>
	3D-ResNet-18	33.2M	11.2	87.5
8-f	3D-ResNeXt-101	48.6M	13.2	86.7
	3D-ResNet-18	33.2M	10.3	86.1
	2D-ResNet-18	11.2M	0.9	80.8
	3D-MobileNetV1 2.0x	13.9M	0.6	81.6
	3D-MobileNetV2 1.0x	2.1M	0.7	85.1
	3D-ShuffleNetV1 2.0x	4.6M	0.7	85.0
	3D-ShuffleNetV2 2.0x	3.9M	0.6	84.2

Table 3. Performance comparison of different video backbones for different clip lengths. For all experiments, SincDSNet is used at the audio backbone. For the evaluations, face crop resolution of  $160 \times 160$  is used.

## 4. Experiments

In this section we validate all the design choices applied at three stages of our ASDNet architecture.

**Dataset.** The AVA-ActiveSpeaker dataset [42] is considered as the first audio-visual active speaker dataset collected in the wild. It contains 262 15-minute videos from Hollywood movies, recorded at 25-30 fps, 120 of which are used for training, 33 for validation, and 109 for testing. The videos consist of 3.65 million human-labeled frames, where face crops belonging to the same speaker are aggregated to create face tracks, and each face crop is annotated with *speaking* or *not-speaking* label. This results in 38.5 hours of face tracks with the corresponding audio signal. The number of speakers in the videos is time-varying, and a significant portion of face crops has resolution less than 100 pixels, making the dataset considerably challenging.

**Evaluation Metric.** We use official ActivityNet evaluation tool that computes mean average precision (mAP). If not stated otherwise, we use AVA-ActiveSpeaker validation set for our evaluations.

### 4.1. Audio-Visual Encoder Evaluation

The performance reported in this section is acquired using only the audio-visual backbones. ISRM and temporal modeling stages are not used in this section.

**Which type of encoder architectures should be selected?** Selection of appropriate encoder architecture is of utmost importance: the overall performance of the AV-ASD pipeline can only be as good as the extracted features. Following recent works [1, 6, 32, 42, 54], we start from a baseline audio-visual encoder that uses 2D-ResNet-18 architecture for the audio and video backbones. We used stacked face crops for the video and MFCC for the audio input to

Number of Background Speakers	mAP
0	92.6
1	93.1
2	<b>93.4</b>
3	<b>93.4</b>
4	<b>93.4</b>
5	93.3

Table 4. Performance comparison of using different number of background speakers. Results are acquired using temporal modeling of Bidirectional-GRU with sequence length of 64.

Method	Temporal Modeling	mAP
NonLocal		87.2
NonLocal	✓	92.8
ISLR (ours)		89.0
ISLR (ours)	✓	<b>93.4</b>

Table 5. Performance comparison of inter-speakers relation modeling methods As temporal modeling method, Bidirectional-GRU with sequence length of 64 is used.

the baseline, with length of 8 frames. This baseline achieves 79.0 mAP as shown in Table 1.

To evaluate the benefit of capturing motion patterns in videos, we replaced the 2D-ResNet-18 backbone (based on 2D-CNNs) with 3D-ResNet-18 (based on 3D-CNNs), while keeping the audio backbone same. This bring almost 5 mAP improvement over the baseline.

To evaluate the benefit of the partially learnable feature extraction by SincDSNet operating on raw audio data, over the existing MFCC + computer vision-based audio backbones, we replaced the audio backbone in the baseline by SincDSNet, while keeping the baseline video backbone. This brings 2 mAP improvement over baseline. Note that SincDSNet has 75 times less parameters than 2D-ResNet-18 and requires less number of floating point operations (FLOPs), as shown in Table 2.

Finally, our proposed audio-visual encoder with SincDSNet and 3D-ResNet-18 backbones, achieves around 7 mAP improvement over the baseline.

**Can we use resource-efficient video encoders?** One can attribute the performance boost achieved by 3D-ResNet-18 backbone to its increased number of parameters and FLOPs. Therefore, we have used several resource efficient 3D CNNs [24] as video backbone and reported their performance at the bottom part of Table 3. It can be seen that all 3D CNN architectures achieve better performance than 2D-ResNet-18. As an example, although 3D-MobileNetV2 1.0x contains much smaller number of parameters (around 7 times less) and smaller FLOPs compared to 2D-ResNet-18,

Background features	mAP
only reference frame	93.4
neighbouring window of 9 frames	<b>93.5</b>

Table 6. Performance comparison when background speakers’ features at different number of frames are leveraged. Bidirectional-GRU with sequence length of 64 is used as temporal modeling.

it achieves around 4 mAP better performance.

We have also experimented with deeper and computationally more expensive 3D-ResNeXt-101 architecture to check how much performance can be increased. 3D-ResNeXt-101 shows 0.6 mAP improvement over 2D-ResNet-18 when 8-frames input is used.

**How does clip length affect performance?** Although we have used 8-frames clips to train our audio-visual backbones, larger clip lengths would be beneficial providing larger temporal support. Therefore, we have compared clip lengths of 8-frames, 16-frames and 32-frames for the best performing 3D-ResNeXt-101 and 2D-ResNet-18 video backbones in Table 3. In order to keep complexity same, we have modified the networks by removing the initial temporal downsampling for 8-frames input, and inserting an additional temporal downsampling to the initial convolution layer for 32-frames input. Applying 16-frames clip length brings a performance improvement of 1.4 mAP and 2.2 mAP over 8-frames clip length for 2D-ResNet-18 and 3D-ResNeXt-101, respectively. Using 32-frames clip length does not show same performance improvement over using 16-frames. We suspect that inserting additional temporal downsampling hinders backbones ability to capture motion patterns.

There is still an open question: How does improvement achieved by increased clip length reflect to the final performance after ISRM and temporal modeling stages? This question is answered in the later sections.

## 4.2. Inter-Speaker Relation Modeling Evaluation

**How many background speakers to use for ISRM?** We have experimented with different number of background speakers at our ISRM shown in Fig. 5 and reported comparative results in Table 4. In general, using larger amount of background speakers’ features increases the performance. Utilization of ISRM increases the performance by 0.8 mAP compared to the case where only reference speaker’s features are used with temporal modeling (0 background speaker case). We stick to using 3 background speakers for the rest of our analyses.

**How does our ISRM compare to existing approaches?** We have compared our ISRM approach with the NonLocal [51] variant proposed in [1] in Table 5. NonLocal variant captures relationships between all the speakers within

Method	Sequence Length	mAP
Bidirectional-GRU	64	<b>93.5</b>
Bidirectional-LSTM	64	93.4
Bidirectional-SRU	64	93.2
GRU	32	92.8
LSTM	32	92.7
SRU	32	92.7

Table 7. Performance comparison of temporal modeling methods.

Sequence Length	mAP
8	92.0
16	92.8
32	93.3
64	<b>93.5</b>
128	<b>93.5</b>

Table 8. Performance comparison of using different sequence lengths at the training of Bidirectional-GRU.

clip, whereas our ISLR approach captures relationships between speakers only within reference frame. When used alone NonLocal approach does not improve performance, even degrades it. Our ISLR approach also does not contribute much performance improvement when used alone. However, it contributes additional 0.8 mAP compared to the case that use only temporal modeling.

**Can ISRM benefit from neighbouring frames?** At ISRM, we do not have to use background speakers’ features at only reference frame. Neighbouring frames relative to the reference frame can also provide useful information for ISRM. Therefore we have used background speakers’ features at neighbouring window of 9 frames, which shows a modest 0.1 mAP improvement as reported in Table 6. For the rest of the paper, we use 9 neighbouring frames at ISRM.

### 4.3. Temporal Modeling Evaluation

**Which RNN architectures are most suitable?** Table 7 shows the performance comparison of different RNN blocks used for temporal modeling. All one-directional methods takes 32-frames features as input and last output is used as input to final fc layer (reference frame is placed to the last of input sequence). For bidirectional methods, we have used 64-frames features as input and center output is used as input to final fc layer (reference frame is placed at the center of input sequence). Compared to their bidirectional versions, one-directional methods perform around 0.7 mAP worse. Out of all methods, bidirectional-GRU achieves the best performance.

**What should be the length of the input sequence?** We have experimented with different sequence lengths and re-

#	Speaker Video Feat.	Audio Feat.	ISRM Feat.	Temporal Modeling	mAP
1	✓				78.8
2		✓			49.3
3	✓	✓			88.9
4	✓	✓		✓	92.6
5	✓	✓	✓		89.6
6		✓	✓		64.5
7		✓	✓	✓	67.8
8	✓	✓	✓	✓	<b>93.5</b>

Table 9. Contribution of each component to the final performance.

Encoder Clip Length	ISRM and Temporal Modeling	mAP
8-frames	✗	86.7
16-frames	✗	88.9
8-frames	✓	93.4
16-frames	✓	93.5

Table 10. Effect of encoder clip length on the final performance.

Order	mAP
ISRM first	<b>93.5</b>
Temporal Modeling first	93.4

Table 11. Performance comparison when the order of ISRM and temporal modeling is changed.

ported results in Table 8. In general, using larger sequence length does not hurt the final performance. However, after sequence length 64, the performance converges to 93.5 mAP.

### 4.4. Component-wise Analysis

#### *How does each component contribute to the performance?*

We have investigated the contribution of each component to the final performance in Table 9. We highlight several findings: (i) Without ISRM and temporal modeling, suitable backbones alone achieves 88.9 mAP, which is better than any other state-of-the-art approaches. (ii) ISRM and temporal modeling improves the performance by 0.7 mAP and 3.7 mAP when they are applied alone, respectively, which shows that both stages are critical in our pipeline. (iii) At lines 6 and 7 in Table 9, we have investigated the importance of ISRM stage by evaluating the performance without using reference speakers video features. Accordingly, even without looking reference speaker’s face, information acquired from background speakers and audio enables our architecture to achieve around 68 mAP. This shows that ISRM is an indispensable part of our pipeline. (iv) When ISRM and temporal modeling are applied together, our architecture achieves the best performance with 93.5 mAP.

	Method	mAP
validation set	ASDNet (ours)	<b>93.5</b>
	Causal ASDNet (ours)	90.6
	MAAS-TAN [32]	88.8
	Chung et al. [6]	87.8
	ASC [1]	87.1
	Zhang et al. [54]	84.0
	Sharma et al. [44]	82.0
	Roth et al. [42]	79.2
test set	ASDNet (ours) *	<b>91.7</b>
	Chung et al. [6]	87.8
	ASC [1]	86.7
	Zhang et al. [54]	83.5
	Roth et al. [42]	82.1

Table 12. Comparison with state-of-the-art methods on the AVA-ActiveSpeaker dataset. \*Test performance of ASDNet is acquired by contacting AVA-ActiveSpeaker dataset providers since the evaluation server was closed at the time of submission.

**How does the clip length affect performance?** Increased encoder clip length improves the performance by 2.2 mAP if ISRM and temporal modeling are not applied. However, in the complete pipeline this improvement reflects to a marginal 0.1 mAP improvement in the final performance, which is shown in Table 10. This shows that increased encoder clip length shifts the improvement that could have been provided by temporal modeling to the encoder. This might not be desirable if complexity is important at the design of the architecture since doubling encoder clip length means doubling the complexity.

**Can ISRM be placed after temporal modelling?** If necessary, the order of ISRM and temporal modeling can be changed, which results in only a 0.1 mAP performance degradation as shown in Table 11.

**Can we make the full pipeline causal?** The complete pipeline can be made causal by placing the reference frame to the last place of the input for encoder and temporal modeling stages; and by not using neighbouring frames background speakers’ features at ISRM. So that, no future information is used for the active speaker detection of the current frame. Causal pipeline achieves 90.6 mAP, which is still better than any state-of-the-art approach.

#### 4.5. Comparison with the State-of-the-art

**How does ASDNet compare to state-of-the-art methods?** We compare the performance of ASDNet with several state-of-the-art methods in Table 12. For the final ASDNet, we used 16-frame clips at the audio-visual encoding stage, 3 background speakers with 9 neighbouring window at the ISRM stage, and bidirectional-GRU with 64-frame clips at

Method	Number of Faces		
	1	2	3
ASDNet (Ours)	<b>95.7</b>	<b>92.4</b>	<b>83.7</b>
MAAS [32]	93.3	85.8	68.2
ASC [1]	91.8	83.8	67.6
Baseline [42]	87.9	71.6	54.4

Table 13. Performance comparison by number of visible faces on each frame.

Method	Face Size		
	S	M	L
ASDNet (Ours)	<b>74.3</b>	<b>89.8</b>	<b>96.3</b>
MAAS [32]	55.2	79.4	93.0
ASC [1]	56.2	79.0	92.2
Baseline [42]	44.9	68.3	86.4

Table 14. Performance comparison by face size.

the temporal modeling stage. ASDNet outperforms the second best approach by 4.7 mAP on the validation set, and by 3.9 mAP on the test set of AVA-ActiveSpeaker dataset.

**How does number of faces affect the performance?** Increased number of faces makes the active speaker detection task more challenging and the performance of ISRM becomes more critical. ASDNet outperforms all other state-of-the-art methods for all different face numbers as shown in Table 13. Superiority of ASDNet becomes more significant as number of faces increases.

**How does face size affect the performance?** Performance comparison for face size, which is set as small for  $[0, 64)$ , medium for  $[64, 128)$ , and large for  $[128, \infty)$  pixels, is shown in Table 14. ASDNet outperforms all other state-of-the-art methods for all different face sizes. Superiority of ASDNet becomes more significant for smaller faces.

## 5. Conclusion

In this paper, we scrutinized the task of Audio-Visual Active Speaker Detection and proposed a three-stage architecture, called ASDNet. ASDNet outperforms the previous state-of-the-art with significant 4.7 mAP and 3.9 mAP on the validation and test set of AVA-ActiveSpeaker dataset, respectively. To design ASDNet, we followed insights from numerous carefully designed experiments that targeted a specific aspect of the system. Each of these experiments was discussed in the paper. We believe that these insights can be useful for other complex audio-visual tasks as well that require context and temporal modeling.



## References

- [1] Juan León Alcázar, Fabian Caba, Long Mai, Federico Perazzi, Joon-Young Lee, Pablo Arbeláez, and Bernard Ghanem. Active speakers in context. In *Proceedings of the IEEE/CVF Conference on Computer Vision and Pattern Recognition*, pages 12465–12474, 2020. 1, 2, 3, 4, 5, 6, 8
- [2] I. Ariav and I. Cohen. An end-to-end multimodal voice activity detection using wavenet encoder and residual networks. *IEEE Journal of Selected Topics in Signal Processing*, 13(2):265–274, 2019. 2
- [3] Joao Carreira and Andrew Zisserman. Quo vadis, action recognition? a new model and the kinetics dataset. In *proceedings of the IEEE Conference on Computer Vision and Pattern Recognition*, pages 6299–6308, 2017. 2, 5
- [4] Punarjay Chakravarty, Sayeh Mirzaei, Tinne Tuytelaars, and Hugo Van hamme. Who’s speaking? audio-supervised classification of active speakers in video. In *Proceedings of the 2015 ACM on International Conference on Multimodal Interaction*, pages 87–90, 2015. 2
- [5] Kyunghyun Cho, Bart Van Merriënboer, Dzmitry Bahdanau, and Yoshua Bengio. On the properties of neural machine translation: Encoder-decoder approaches. *arXiv preprint arXiv:1409.1259*, 2014. 4
- [6] Joon Son Chung. Naver at activitynet challenge 2019–task b active speaker detection (ava). *arXiv preprint arXiv:1906.10555*, 2019. 3, 4, 5, 8
- [7] Joon Son Chung, Arsha Nagrani, and Andrew Zisserman. Voxceleb2: Deep speaker recognition. *Proc. Interspeech 2018*, pages 1086–1090, 2018. 1
- [8] Gabriella Csurka, Christopher Dance, Lixin Fan, Jutta Willamowski, and Cédric Bray. Visual categorization with bags of keypoints. In *Workshop on statistical learning in computer vision, ECCV*, volume 1, pages 1–2. Prague, 2004. 2
- [9] Ross Cutler and Larry Davis. Look who’s talking: Speaker detection using video and audio correlation. In *2000 IEEE International Conference on Multimedia and Expo. ICME2000. Proceedings. Latest Advances in the Fast Changing World of Multimedia (Cat. No. 00TH8532)*, volume 3, pages 1589–1592. IEEE, 2000. 1, 2
- [10] Trevor Darrell, John W Fisher, and Paul Viola. Audio-visual segmentation and “the cocktail party effect”. In *International Conference on Multimodal Interfaces*, pages 32–40. Springer, 2000. 1, 2
- [11] Jia Deng, Wei Dong, Richard Socher, Li-Jia Li, Kai Li, and Li Fei-Fei. Imagenet: A large-scale hierarchical image database. In *2009 IEEE conference on computer vision and pattern recognition*, pages 248–255. Ieee, 2009. 2, 5
- [12] Sander Dieleman and Benjamin Schrauwen. End-to-end learning for music audio. In *2014 IEEE International Conference on Acoustics, Speech and Signal Processing (ICASSP)*, pages 6964–6968. IEEE, 2014. 2
- [13] Ariel Ephrat, Inbar Mosseri, Oran Lang, Tali Dekel, Kevin Wilson, Avinatan Hassidim, William T. Freeman, and Michael Rubinstein. Looking to listen at the cocktail party: A speaker-independent audio-visual model for speech separation. *ACM Trans. Graph.*, July 2018. 2
- [14] Christoph Feichtenhofer, Haoqi Fan, Jitendra Malik, and Kaiming He. Slowfast networks for video recognition. In *Proceedings of the IEEE/CVF International Conference on Computer Vision*, pages 6202–6211, 2019. 2
- [15] Ruohan Gao, Tae-Hyun Oh, Kristen Grauman, and Lorenzo Torresani. Listen to look: Action recognition by previewing audio. In *Proceedings of the IEEE/CVF Conference on Computer Vision and Pattern Recognition*, pages 10457–10467, 2020. 1
- [16] Israel D Gebru, Sileye Ba, Xiaofei Li, and Radu Horaud. Audio-visual speaker diarization based on spatiotemporal bayesian fusion. *IEEE transactions on pattern analysis and machine intelligence*, 40(5):1086–1099, 2017. 1
- [17] Kensho Hara, Hirokatsu Kataoka, and Yutaka Satoh. Can spatiotemporal 3d cnns retrace the history of 2d cnns and imagenet? In *Proceedings of the IEEE conference on Computer Vision and Pattern Recognition*, pages 6546–6555, 2018. 2
- [18] John R Hershey, Zhuo Chen, Jonathan Le Roux, and Shinji Watanabe. Deep clustering: Discriminative embeddings for segmentation and separation. In *2016 IEEE International Conference on Acoustics, Speech and Signal Processing (ICASSP)*, pages 31–35. IEEE, 2016. 1
- [19] Sepp Hochreiter and Jürgen Schmidhuber. Long short-term memory. *Neural computation*, 9(8):1735–1780, 1997. 4
- [20] Shuiwang Ji, Wei Xu, Ming Yang, and Kai Yu. 3d convolutional neural networks for human action recognition. *IEEE transactions on pattern analysis and machine intelligence*, 35(1):221–231, 2012. 2
- [21] Andrej Karpathy, George Toderici, Sanketh Shetty, Thomas Leung, Rahul Sukthankar, and Li Fei-Fei. Large-scale video classification with convolutional neural networks. In *Proceedings of the IEEE conference on Computer Vision and Pattern Recognition*, pages 1725–1732, 2014. 2
- [22] Diederik P Kingma and Jimmy Ba. Adam: A method for stochastic optimization. *arXiv preprint arXiv:1412.6980*, 2014. 5
- [23] Okan Köpüklü, Fabian Herzog, and Gerhard Rigoll. Comparative analysis of cnn-based spatiotemporal reasoning in videos. *arXiv preprint arXiv:1909.05165*, 2019. 2
- [24] Okan Kopuklu, Neslihan Kose, Ahmet Gunduz, and Gerhard Rigoll. Resource efficient 3d convolutional neural networks. In *Proceedings of the IEEE/CVF International Conference on Computer Vision Workshops*, pages 0–0, 2019. 2, 4, 6
- [25] Okan Kopuklu, Neslihan Kose, and Gerhard Rigoll. Motion fused frames: Data level fusion strategy for hand gesture recognition. In *Proceedings of the IEEE Conference on Computer Vision and Pattern Recognition Workshops*, pages 2103–2111, 2018. 2
- [26] Alex Krizhevsky, Ilya Sutskever, and Geoffrey E Hinton. Imagenet classification with deep convolutional neural networks. *Advances in neural information processing systems*, 25:1097–1105, 2012. 2
- [27] Ludwig Kürzinger, Nicolas Lindae, Palle Klewitz, and Gerhard Rigoll. Lightweight end-to-end speech recognition from raw audio data using sinc-convolutions. *Proc. Interspeech 2020*, pages 1659–1663, 2020. 2, 4
- [28] Ivan Laptev. On space-time interest points. *International journal of computer vision*, 64(2-3):107–123, 2005. 2

- [29] Ivan Laptev, Marcin Marszałek, Cordelia Schmid, and Benjamin Rozenfeld. Learning realistic human actions from movies. In *2008 IEEE Conference on Computer Vision and Pattern Recognition*, pages 1–8. IEEE, 2008. 2
- [30] Jongpil Lee, Taejun Kim, Jiyoung Park, and Juhan Nam. Raw waveform-based audio classification using sample-level cnn architectures. *arXiv preprint arXiv:1712.00866*, 2017. 2
- [31] Tao Lei, Yu Zhang, Sida I. Wang, Hui Dai, and Yoav Artzi. Simple recurrent units for highly parallelizable recurrence. In *Empirical Methods in Natural Language Processing (EMNLP)*, 2018. 4
- [32] Juan León-Alcázar, Fabian Caba Heilbron, Ali Thabet, and Bernard Ghanem. Maas: Multi-modal assignation for active speaker detection. *arXiv preprint arXiv:2101.03682*, 2021. 1, 2, 3, 4, 5, 8
- [33] Chang-Le Liu, Sze-Wei Fu, You-Jin Li, Jen-Wei Huang, Hsin-Min Wang, and Yu Tsao. Multichannel speech enhancement by raw waveform-mapping using fully convolutional networks. *IEEE/ACM Transactions on Audio, Speech, and Language Processing*, 28:1888–1900, 2020. 2
- [34] Joanna Materzynska, Guillaume Berger, Ingo Bax, and Roland Memisevic. The jester dataset: A large-scale video dataset of human gestures. In *Proceedings of the IEEE/CVF International Conference on Computer Vision Workshops*, pages 0–0, 2019. 2
- [35] Qiguang Miao, Yunan Li, Wanli Ouyang, Zhenxin Ma, Xin Xu, Weikang Shi, and Xiaochun Cao. Multimodal gesture recognition based on the resc3d network. In *Proceedings of the IEEE International Conference on Computer Vision Workshops*, pages 3047–3055, 2017. 2
- [36] Simon Mittermaier, Ludwig Kürzinger, Bernd Waschneck, and Gerhard Rigoll. Small-footprint keyword spotting on raw audio data with sinc-convolutions. In *ICASSP 2020-2020 IEEE International Conference on Acoustics, Speech and Signal Processing (ICASSP)*, pages 7454–7458. IEEE, 2020. 2
- [37] Mathew Monfort, Alex Andonian, Bolei Zhou, Kandan Ramakrishnan, Sarah Adel Bargal, Tom Yan, Lisa Brown, Quanfu Fan, Dan Gutfreund, Carl Vondrick, et al. Moments in time dataset: one million videos for event understanding. *IEEE transactions on pattern analysis and machine intelligence*, 42(2):502–508, 2019. 2
- [38] Arsha Nagrani, Chen Sun, David Ross, Rahul Sukthankar, Cordelia Schmid, and Andrew Zisserman. Speech2action: Cross-modal supervision for action recognition. In *Proceedings of the IEEE/CVF Conference on Computer Vision and Pattern Recognition*, pages 10317–10326, 2020. 1
- [39] Florent Perronnin, Jorge Sánchez, and Thomas Mensink. Improving the fisher kernel for large-scale image classification. In *European conference on computer vision*, pages 143–156. Springer, 2010. 2
- [40] Zhaofan Qiu, Ting Yao, and Tao Mei. Learning spatio-temporal representation with pseudo-3d residual networks. In *proceedings of the IEEE International Conference on Computer Vision*, pages 5533–5541, 2017. 2
- [41] Mirco Ravanelli and Yoshua Bengio. Speaker recognition from raw waveform with sincnet. In *2018 IEEE Spoken Language Technology Workshop (SLT)*, pages 1021–1028. IEEE, 2018. 2, 4
- [42] Joseph Roth, Sourish Chaudhuri, Ondrej Klejch, Radhika Marvin, Andrew Gallagher, Liat Kaver, Sharadh Ramaswamy, Arkadiusz Stopczynski, Cordelia Schmid, Zhonghua Xi, et al. Ava active speaker: An audio-visual dataset for active speaker detection. In *ICASSP 2020-2020 IEEE International Conference on Acoustics, Speech and Signal Processing (ICASSP)*, pages 4492–4496. IEEE, 2020. 1, 2, 3, 4, 5, 8
- [43] Olga Russakovsky, Jia Deng, Hao Su, Jonathan Krause, Sanjeev Satheesh, Sean Ma, Zhiheng Huang, Andrej Karpathy, Aditya Khosla, Michael Bernstein, et al. Imagenet large scale visual recognition challenge. *International journal of computer vision*, 115(3):211–252, 2015. 2
- [44] Rahul Sharma, Krishna Somandepalli, and Shrikanth Narayanan. Crossmodal learning for audio-visual speech event localization. *arXiv preprint arXiv:2003.04358*, 2020. 8
- [45] Karen Simonyan and Andrew Zisserman. Two-stream convolutional networks for action recognition in videos. In *Proceedings of the 27th International Conference on Neural Information Processing Systems-Volume 1*, pages 568–576, 2014. 2, 3
- [46] Daniel Stoller, Sebastian Ewert, and Simon Dixon. Wave-u-net: A multi-scale neural network for end-to-end audio source separation. In *Proceedings of the 19th International Society for Music Information Retrieval Conference, ISMIR 2018, Paris, France, September 23-27, 2018*, pages 334–340, 2018. 1
- [47] Du Tran, Lubomir Bourdev, Rob Fergus, Lorenzo Torresani, and Manohar Paluri. Learning spatiotemporal features with 3d convolutional networks. In *Proceedings of the IEEE international conference on computer vision*, pages 4489–4497, 2015. 2
- [48] Du Tran, Heng Wang, Lorenzo Torresani, Jamie Ray, Yann LeCun, and Manohar Paluri. A closer look at spatiotemporal convolutions for action recognition. In *Proceedings of the IEEE conference on Computer Vision and Pattern Recognition*, pages 6450–6459, 2018. 2
- [49] Heng Wang and Cordelia Schmid. Action recognition with improved trajectories. In *Proceedings of the IEEE international conference on computer vision*, pages 3551–3558, 2013. 2
- [50] Quan Wang, Hannah Muckenhirn, Kevin Wilson, Prashant Sridhar, Zelin Wu, John R Hershey, Rif A Saurous, Ron J Weiss, Ye Jia, and Ignacio Lopez Moreno. Voicefilter: Targeted voice separation by speaker-conditioned spectrogram masking. *Proc. Interspeech 2019*, pages 2728–2732, 2019. 2
- [51] Xiaolong Wang, Ross Girshick, Abhinav Gupta, and Kaiming He. Non-local neural networks. In *Proceedings of the IEEE conference on computer vision and pattern recognition*, pages 7794–7803, 2018. 6
- [52] Bing Xu, Naiyan Wang, Tianqi Chen, and Mu Li. Empirical evaluation of rectified activations in convolutional network. *arXiv preprint arXiv:1505.00853*, 2015. 4

- [53] Neil Zeghidour, Nicolas Usunier, Iasonas Kokkinos, Thomas Schaiz, Gabriel Synnaeve, and Emmanuel Dupoux. Learning filterbanks from raw speech for phone recognition. In *2018 IEEE international conference on acoustics, speech and signal Processing (ICASSP)*, pages 5509–5513. IEEE, 2018. 4
- [54] Yuan-Hang Zhang, Jingyun Xiao, Shuang Yang, and Shiguang Shan. Multi-task learning for audio-visual active speaker detection. 3, 4, 5, 8